AFRL-AFOSR-JP-TR-2018-0058

Antimonide-Based III-V Ternary Nanowire Materials for High Performance Infrared Photodetector Applications

Lan Fu
AUSTRALIAN NATIONAL UNIVERSITY RESEARCH OFFICE ACTON (AUSTRALIA)

06/18/2018
Final Report

DISTRIBUTION A: Distribution approved for public release.

Air Force Research Laboratory
AF Office Of Scientific Research (AFOSR)/ IOA
Arlington, Virginia 22203
Air Force Materiel Command

DISTRIBUTION A: Distribution approved for public release.

REPORT DOCUMENTATION PAGE

Form Approved
OMB No. 0704-0188

The public reporting burden for this collection of information is estimated to average 1 hour per response, including the time for reviewing instructions, searching existing data sources, gathering and maintaining the data needed, and completing and reviewing the collection of information. Send comments regarding this burden estimate or any other aspect of this collection of information, including suggestions for reducing the burden, to Department of Defense, Executive Services, Directorate (0704-0188). Respondents should be aware that notwithstanding any other provision of law, no person shall be subject to any penalty for failing to comply with a collection of information if it does not display a currently valid OMB control number.
PLEASE DO NOT RETURN YOUR FORM TO THE ABOVE ORGANIZATION.

1. REPORT DATE *(DD-MM-YYYY)*	2. REPORT TYPE	3. DATES COVERED *(From - To)*
24-07-2018	Final	21 Sep 2016 to 20 Mar 2018

4. TITLE AND SUBTITLE
Antimonide-Based III-V Ternary Nanowire Materials for High Performance Infrared Photodetector Applications

5a. CONTRACT NUMBER

5b. GRANT NUMBER
FA2386-16-1-4076

5c. PROGRAM ELEMENT NUMBER
61102F

6. AUTHOR(S)
Lan Fu, Chennupati Jagadish

5d. PROJECT NUMBER

5e. TASK NUMBER

5f. WORK UNIT NUMBER

7. PERFORMING ORGANIZATION NAME(S) AND ADDRESS(ES)
AUSTRALIAN NATIONAL UNIVERSITY RESEARCH OFFICE ACTON (AUSTRALIA)
CHANCELRY BLDG 10B LG EAST RD
ACTON, 200 AU

8. PERFORMING ORGANIZATION REPORT NUMBER

9. SPONSORING/MONITORING AGENCY NAME(S) AND ADDRESS(ES)
AOARD
UNIT 45002
APO AP 96338-5002

10. SPONSOR/MONITOR'S ACRONYM(S)
AFRL/AFOSR IOA

11. SPONSOR/MONITOR'S REPORT NUMBER(S)
AFRL-AFOSR-JP-TR-2018-0058

12. DISTRIBUTION/AVAILABILITY STATEMENT
A DISTRIBUTION UNLIMITED: PB Public Release

13. SUPPLEMENTARY NOTES

14. ABSTRACT
The PI has had very good success in this basic research grant. They were able to achieve MOCVD growth of good quality GaAsSb/InP core-shell materials, demonstrated the fabrication of GaAsSb core-only and GaAsSb/InP core-shell single NW photodetectors, and characterized and compared GaAsSb core-only and GaAsSb/InP core-shell single NW photodetectors, demonstrating much improved detector performance using GaAsSb/InP core-shell NWs. They have also successfully grown a series of GaAsSb nanowire arrays with different NW diameters and pitches and fabricated nanowire array photodetectors and obtain preliminary data. The PI has 1 peer reviewed paper in submission, and 3 conference presentations as a direct result of the grant.

15. SUBJECT TERMS
Metal-Organic Chemical Vapor Deposition (MOCVD), Nanofabrication, Nanowires, Core-Shell Alloys, Bandgap, Tunable Absorption

16. SECURITY CLASSIFICATION OF:			17. LIMITATION OF ABSTRACT	18. NUMBER OF PAGES	19a. NAME OF RESPONSIBLE PERSON
a. REPORT	b. ABSTRACT	c. THIS PAGE			CHEN, JERMONT
Unclassified	Unclassified	Unclassified	SAR		19b. TELEPHONE NUMBER *(Include area code)* 315-227-7007

Standard Form 298 (Rev. 8/98)
Prescribed by ANSI Std. Z39.18

DISTRIBUTION A: Distribution approved for public release.

Report (Project FA2386-16-1-4076)

Antimonide-based III–V ternary NW materials for high performance infrared photodetector applications

Principal Investigators: A/Prof. Lan Fu and Prof. Chennupati Jagadish
Key Researcher(s): Dr. Ziyuan Li, Dr. Qian Gao (PhD award June, 2017)
Affiliation of each Researcher(s): Department of Electronic Materials Engineering, Research School of Physics and Engineering, The Australian National University, Canberra, ACT 2601, Australia
Period-of-Performance: Sept., 2016 – Aug., 2017
Extension period: Sept. 2017 – March. 2018

Since the start of the research project from Sept. 2016, the project has progressed very well as originally planned:

1. For the proposed research on **GaAsSb/InP single nanowire infrared photodetectors**, we have achieved:

- MOCVD growth of good quality GaAsSb/InP core-shell materials
- Fabrication of GaAsSb core-only and GaAsSb/InP core-shell single NW photodetectors
- Characterisation and comparison between GaAsSb core-only and GaAsSb/InP core-shell single NW photodetectors, demonstrating much improved detector performance using GaAsSb/InP core-shell NWs.

The experimental work of this project has been all finished. We are in the process of finalising the data analysis and manuscript preparation. A draft manuscript including most of the results has been attached as "**Summary: Project 1**".

2. For the proposed research on **GaAsSb nanowire array infrared photodetectors**, we have successfully grown a series of GaAsSb nanowire arrays with different NW diameters and pitches. We have also fabricated nanowire array photodetectors and obtain preliminary data, as summarised in "**Summary: Project 2**".

Due to the leaving of our nanowire grower (Dr. Qian Gao) to take up a new job, as well as a few short delays due to key experimental equipment broken down or maintenance (MOCVD reactor, PECVD, and sputter coating system), our planned research on GaAsSb nanowire array photodetectors has not been completed yet. We have been granted a 6-month extension to finalize our experimental/simulation work on GaAsSb nanowire array photodetectors to obtain sufficient data for a new research paper.

During the extension period from Sept. 2017 – March 2018:

1. We have been focusing on finalising the experimental work on GaAsSb nanowire array detectors and also collaborating with Drs. Jeffery Allen, Monica Allen and Simeon Trendafilov on optical simulation of the array absorption. The optical simulation results agree well with our experimental data and also provide further important guidance on array geometry optimisation to achieve wider tenability of our GaAsSb array photodetectors ranging for visible to near infrared. Based on the simulation results, we are very keen to grow and fabricate another batch of GaAsSb nanowire

DISTRIBUTION A: Distribution approved for public release.

arrays to extend the current detection peak wavelength from 400nm to beyond 1100nm, which we believe will lead to higher quality/impact publications. To summarise, for GaAsSb nanowire array photodetector work, we have achieved:

- MOCVD growth of good quality GaAsSb array nanowires with different NW diameters of 30nm, 50nm, 70nm and 100nm and nanowire spacing of 400nm and 800nm respectively.
- Fabrication and characterisation of GaAsSb array NW photodetectors, demonstrating good photodetector performance with peak spectral response from 400nm - 800nm.
- Collaboration with US air force partners to understand the nanowire array absorption properties to explain the experimental data and design new array geometry to achieve the multispectral photodetection with a wide spectral tunability for a broad range of applications.

The experimental and simulation results we have obtained so far have been drafted in a manuscript "**Room temperature GaAsSb nanowire array photodetectors**" (see attachment 1). We hope to finish our final experiments and add the data to improve the manuscript.

2. The manuscript on the GaAsSb/InP core-shell photodetector have been drafted and entitled as "**GaAsSb/InP core-shell single nanowire infrared photodetectors**" (see attachment 2), which is currently under further improvement - we have also decided to add an extra experiment on ammonia sulphur plus SiN passivation for comparison to strengthen the paper.

Finally, together with the report, we have also attached three conference abstract/summaries for SPIE NanoPhotonics Australasia 2017, Melbourne, Australia (oral presentation), ICONN 2018, Wollongong, Australia (oral presentation), RAPID, Florida, USA (oral presentation) based on this project.

DISTRIBUTION A: Distribution approved for public release.

Room temperature GaAsSb nanowire array photodetectors

Ziyuan Li[1], Simeon Trendafilov[2], Monica Allen[2], Jeffery Allen[2], Ahmed Alabadla[1], Qian Gao[1], Xiaoming Yuan[1,3], Inseok Yang[1], Philippe Caroff[1,4], Hark Hoe Tan[1], Chennupati Jagadish[1] and Lan Fu[1]

[1] Department of Electronic Materials Engineering, Research School of Physics and Engineering, The Australian National University, Canberra, ACT 2601, Australia

[2] Air Force Research Laboratory, Munitions Directorate, Eglin AFB, FL 32542, USA

[3] School of Physics and Electronics, Hunan Key Laboratory for Supermicrostructure and Ultrafast Process, Central South University, 932 South Lushan Road, Changsha, Hunan 410083, P. R. China

[4] Microsoft Station Q, Delft University of Technology, Building 22, Faculty of Applied Sciences, Lorentzweg 1, 2628 CJ Delft, Netherlands

Email: jeffery.allen.12@us.af.mil, lan.fu@anu.edu.au

Abstract

Ternary III-V semiconductor nanowires (NWs) such as $GaAs_xSb_{1-x}$ NWs have been demonstrated as potential candidates for nanoscale optoelectronics applications due to their high photoresponse and tunable bandgap over a wide range. In this work, $GaAs_{0.94}Sb_{0.06}$ NW arrays were successfully grown along the <111>A direction with high uniformity by gold-seeded metalorganic vapor phase epitaxy (MOVPE) and fabricated as room temperature high performance photodetectors. It was found that the NW morphology, optical property as well as photodetection performance could be well controlled by the gold-seed shape and position. Such GaAsSb NW array photodetectors present tunable resonance peaks varying with the NW geometry and array pitch, showing photocurrent responsivity as high as 27 A/W@1V. Simulated light absorption spectra confirm the strong resonance modes supported in the NWs due to their waveguiding properties. These devices are promising for future multispectral photodetector applications.

Keywords: GaAsSb, III-V semiconductor, nanowire, VLS, photodetector

1. Introductions

Ternary III-V semiconductor nanowires (NWs) are of increasing interest in recent years due to their small footprint, wide tunable bandgap, unique optical and electrical properties, which can be applied in

DISTRIBUTION A: Distribution approved for public release.

optoelectronic applications such as photodetectors [1-4], solar cells [5-7] and transistors [1, 2, 8]. In particular, $GaAs_xSb_{1-x}$ NWs have been intensively studied including their growth mechanism, optical properties, band gap engineering, surface passivation as well as potential applications [1-3, 9-11]. Currently, the $GaAs_xSb_{1-x}$ NWs are mainly grown by using metal-catalyzed or self-catalyzed vapor-liquid-solid (VLS) techniques [9, 11]. Especially, metal-seeded III-V NWs have played important roles within the semiconductor NW family due to their maturity in controlled growth, providing high crystal quality materials with excellent properties such as high carrier mobility, superior optical properties as well as flexibility of bandgap engineering [10-15]. Moreover, due to the contact with the growing crystal and its environment, the seed particles could be directly linked to the growth control of metal-seeded NWs through the choice of metal, their alloy composition, shape, physical state and spatial configuration [15, 16].

In this work, the NWs were grown by a metalorganic vapor phase epitaxy (MOVPE) reactor based on gold-seeded VLS technique. We thoroughly studied the impact of the gold-seed diameter on the NW morphology, optical properties and photodetection performance when the NW array's pitch size is 400 nm and 800 nm, respectively. The seed diameter was controlled through a selective-area lift-off process by using electron-beam lithography (EBL) and electron-beam gold deposition. A SiO_2 layer mask was used to accurately define the size and position of gold-seeds and thus NWs as well as to suppress parasitic growth. Without the SiO_2 mask, the density of NWs would be much smaller with varied lengths [15]. The photoconductive devices based on such NW arrays display diode-like current-voltage (*I-V*) characteristics and high photoresponse with tunable resonances. The results indicate their promising application as photodetectors for the next-generation multispectral photodetection systems. It is believed that the results and interpretation given here could also be valid for the other metal-seeded III–V NW material systems.

2. Experiments

DISTRIBUTION A: Distribution approved for public release.

A. Synthesis and characterization of $GaAs_xSb_{1-x}$ NWs

$GaAs_xSb_{1-x}$ NW arrays were grown by using a horizontal flow MOVPE reactor (Aixtron 200/4) at 100 mbar based on the gold-seeded VLS technique. In order to obtain gold colloids with diameter size of 30, 50, 70 and 100 nm, respectively, a 30 nm SiO_2 layer was first deposited on a p-type (111)A GaAs substrate by using plasma-enhanced chemical vapor deposition (PECVD), followed by EBL patterning to define the hole diameter and array pitch. The wet etching using 1% HF for 75 s was conducted to open the holes in the SiO_2 layer. Then the gold particles were obtained after the electron-beam evaporation of a 17 nm gold layer and a lift-off process. After that, the substrate was loaded into the reactor where $GaAs_xSb_{1-x}$ NW arrays were grown at 500 °C with Trimethylgallium (TMGa), trimethylantimony (TMSb) and arsine (AsH_3) as precursors for Ga, Sb and As with a flow of 0.9×10^{-5}, 1.2×10^{-5} and 1.35×10^{-5} mol/min, respectively. The morphology of $GaAs_xSb_{1-x}$ NW arrays were characterized by a scanning electron microscope (SEM) and the overall Sb composition was measured by an energy dispersive X-ray (EDX) spectroscopy equipped in a transmission electron microscope (TEM). Their optical properties were assessed by room-temperature micro-photoluminescence (μ-PL) using a confocal micro-Raman system (Horiba Jobin Yvon 64000) equipped with a laser diode emitting at 532 nm.

B. Device fabrication and measurements

After growth, the NW arrays were fabricated into photodetectors through processes of photoresist planarization (AZ 5214E), barrel etching using oxygen plasma to free the nanowire tips, wet etching using HF or HCl to remove the native oxide and transparent conducting layer (e.g. indium tin oxide (ITO)) deposition on front side and metal contact deposition on back side. The typical dark/light *I-V* curves of the NW detectors were measured by a 2420 SourceMeter® when the light source was provided by a 1 Sun solar simulator. The photocurrent spectral response of the detectors was measured using the conventional amplitude modulation technique with a tungsten-halogen lamp as a white illumination

DISTRIBUTION A: Distribution approved for public release.

source, a mechanical chopper, an Acton SpectraPro® 2300i monochromator, a Stanford SR570 low-noise current pre-amplifier and a Stanford SR830 DSP lock-in amplifier [2].

3. Results and discussion

Figure 1 shows the SEM images of the as-grown $GaAs_xSb_{1-x}$ NW arrays with pitch size (P) of 400 and 800 nm and gold particle diameter (D) of 30, 50, 70 and 100 nm, respectively. All the NWs reveal a nearly 100% vertical yield along the [111]A direction with significantly high uniformity. When D is small (e.g., 30 nm), the NWs show a certain degree of tapering due to a large simultaneous lateral growth. When the NW diameter is increasing as result of larger gold particle size, less tapering degree but slightly shorter length were observed. The NWs in the arrays with P of 800 nm present longer length (1.8-2.1 μm) than those NWs in the arrays with P of 400 nm (1.4-1.6 μm) because of more adatoms on the oxide mask diffusing to the top of the NWs and participating in the axial growth. The $GaAs_xSb_{1-x}$ NWs present high crystal quality with a twin-free zinc blende (ZB) structure, as demonstrated by the TEM images together with the high resolution TEM (HRTEM) image of a selected region and corresponding diffraction pattern in Figure 2. It is observed that Au droplet has moved to the inclined sidewall of the NW during cooling down, suggesting that the NW growth is not under a steady condition [15]. A uniform composition profile along the NW axis was confirmed by the EDX line scan and the Sb concentration was calculated to be ~ 6%. In comparison to the low Sb composition in the NW, high Sb content was found in the Au droplet, indicating a low incorporation ratio of the Sb during the NW nucleation. Consequently, large Sb content in the NW could be challenging to achieve.

Figure 3 presents the PL spectra of these $GaAs_{0.94}Sb_{0.06}$ NW arrays with P of (a) 400 and (b) 800 nm, respectively. Arrays with P of 400 nm show averagely larger PL intensity because of their larger NW density under the same light illumination. As clearly seen in Fig. 3(a), the NW array with D=100 nm and P=400 nm shows an apparent peak at wavelength of ~ 1100 nm with the highest PL intensity, while the NW array with D=30 nm shows much lower PL peak intensity with a red-shifted band gap, which may

DISTRIBUTION A: Distribution approved for public release.

be due to the decreased material volume, degraded material quality, and/or slightly increased Sb composition. The PL spectra of arrays with P of 800 nm indicate the same trend but less degree as shown in Fig. 3(b). The significantly enhanced PL signal below 1000 nm was demonstrated to be from the GaAs substrate by PL measurements on single horizontal $GaAs_{0.94}Sb_{0.06}$ NWs.

In order to characterize the performance of the NW array photodetectors, dark/light *I-V* characteristics as plotted in Figure 4 were first obtained. To get the light *I-V* curves, the whole arrays were under 1 Sun light illumination. It was supposed that the forward bias voltage was applied at the gold back side of the NW arrays. Clearly seen, all the *I-V* curves present a diode behavior. It is probably due to the Schottky contact formed between GaAsSb NWs (unintentionally p-type doped) and ITO (n-type). All arrays show much higher light currents than dark currents under the forward bias, indicating their good photocurrent response. The NW array with D=100 nm clearly shows highest light current while its dark current is lowest, indicating its best photoresponse. As we expected, NW arrays with smaller size of D produce less photocurrent due to decreased material volume. Pitch size of 800 nm shows the same trend as pitch size of 400 nm but with less degree.

Figure 5 presents the photocurrent response of the NW array photodetectors under a bias voltage of 1 V when the white light spot size is 11 μm. It can be seen that larger D leads to higher photocurrent response but shortened current tail, which is consistent with the PL results. In particular, such GaAsSb NW arrays show a strong resonance in the wavelengths much shorter than the NW bandgap, with an increased blue shift with the decrease of NW diameter. This is because that NWs exhibit strong waveguiding properties and efficiently couple incident light to resonant modes supported in the NWs. Since our GaAsSb NWs have relatively small diameters, short wavelength light can be easily coupled to strong resonance modes, leading to significantly enhanced photoresponse. The photodetectors' spectral responsivity (R) was calculated by:

$$R = I_{ph} / P_{in}, \quad (1)$$

DISTRIBUTION A: Distribution approved for public release.

where I_{ph} is the photocurrent and P_{in} is the light power incident onto the NW arrays. The responsivity of the NW array with D of 100 nm and P of 400 nm can reach as high as 27 A/W at the peak wavelength of 480 nm. The photoresponse of arrays with P of 800 nm also show strong resonances in short wavelengths with blue-shifted peak for smaller NW diameter. The responsivity of the NW array with D of 100 nm and P of 800 nm is about 10.3 A/W at the peak wavelength of 505 nm. It is less than that of the arrays with P of 400 nm due to the much less NW density.

To further understand the reason why the $GaAs_{0.94}Sb_{0.06}$ NW array photodetectors have such strong resonances, the optical absorption properties of these arrays were simulated using COMSOL Multiphysics as shown in Figure 6. As clearly seen from Figs. 6(a) and (b), the NWs have very strong absorption in the wavelengths much shorter than their bandgap, with an increased blue shift and lower absorption efficiency with the decrease of NW diameter when D is ranging from 30 to 100 nm. Based on the morphology shown in the SEM images (Fig. 1), the GaAsSb nanorods are tapered by 10% at the top in the simulations. Moreover, larger pitch size with the same NW diameter would lead to resonance red-shift as also indicated in the photocurrent spectra. In order to confirm the resonance tunability of our $GaAs_{0.94}Sb_{0.06}$ NW arrays, the absorption spectra for arrays with larger D ranging from 120 to 240 nm when P=800 nm are also simulated separately (Fig. 6(c)), clearing showing strong resonances with a peak wavelength shift towards near-infrared when D is increased. In these diameter ranges, since it is less tapering, the GaAsSb nanorods are tapered by 5% at the top in the simulations. It is demonstrated that, with proper design of NW arrays regrading to the NW diameter and array pitch, we are able to achieve high performance $GaAs_{0.94}Sb_{0.06}$ photodetectors with a wide spectral tunability for future multispectral photodetection.

4. Conclusions

In summary, $GaAs_{0.94}Sb_{0.06}$ NW arrays with tunable diameter and pitch size were synthesized using MOVPE and successfully demonstrated to operate as high performance photodetectors at room

DISTRIBUTION A: Distribution approved for public release.

temperature. It is demonstrated that by engineering the diameter and pitch size of the gold-seeds, $GaAs_{0.94}Sb_{0.06}$ NWs showed tunable morphology and photodetection performance. Furthermore, the $GaAs_{0.94}Sb_{0.06}$ NW array photodetectors show strong and wavelength-tunable resonances in both visible and near-infrared ranges with high photoreponse. Therefore, it is promising to achieve multispectral photodetection with a wide spectral tunability highly desirable for a broad range of applications by further design and fabrication of NW arrays with different geometries (diameter and spacing).

Acknowledgments

The authors would like to acknowledge the support from the Air Force Office of Scientific Research (AFOSR) (PO: Dr. J. Chen; FA2386-16-1-4076) and Australian Research Council (ARC). The authors (MSA and JWA) are thankful for the funding support through AFOSR Lab Task 17RWCOR398 (PO: Dr. K. Caster) and Air Force Research Laboratory (AFRL) Munitions Directorate Chief Scientist (Dr. D. Lambert). The facility support from the Australian National Fabrication Facility (ANFF) ACT node is also acknowledged.

References

[1] Huh J, Yun H, Kim D-C, Munshi A M, Dheeraj D L, Kauko H, van Helvoort A T, Lee S, Fimland B-O and Weman H 2015 Rectifying single GaAsSb nanowire devices based on self-induced compositional gradients *Nano Letters* **15** 3709-15

[2] Li Z, Yuan X, Fu L, Peng K, Wang F, Fu X, Caroff P, White T P, Tan H H and Jagadish C 2015 Room temperature GaAsSb single nanowire infrared photodetectors *Nanotechnology* **26** 445202

[3] Ma L, Zhang X, Li H, Tan H, Yang Y, Xu Y, Hu W, Zhu X, Zhuang X and Pan A 2015 Bandgap-engineered GaAsSb alloy nanowires for near-infrared photodetection at 1.31 μm *Semiconductor Science and Technology* **30** 105033

[4] Tan H, Fan C, Ma L, Zhang X, Fan P, Yang Y, Hu W, Zhou H, Zhuang X and Zhu X 2016 Single-crystalline InGaAs nanowires for room-temperature high-performance near-infrared photodetectors *Nano-Micro Letters* **8** 29-35

[5] Gutsche C, Lysov A, Braam D, Regolin I, Keller G, Li Z A, Geller M, Spasova M, Prost W and Tegude F J 2012 n‐GaAs/InGaP/p‐GaAs Core‐Multishell Nanowire Diodes for Efficient Light‐to‐Current Conversion *Advanced Functional Materials* **22** 929-36

[6] Holm J V, Jørgensen H I, Krogstrup P, Nygård J, Liu H and Aagesen M 2013 Surface-passivated GaAsP single-nanowire solar cells exceeding 10% efficiency grown on silicon *Nature Communications* **4** 1498

[7] Nakai E, Chen M, Yoshimura M, Tomioka K and Fukui T 2014 InGaAs axial-junction nanowire-array solar cells *Japanese Journal of Applied Physics* **54** 015201

DISTRIBUTION A: Distribution approved for public release.

[8] Hou J J, Han N, Wang F, Xiu F, Yip S, Hui A T, Hung T and Ho J C 2012 Synthesis and characterizations of ternary InGaAs nanowires by a two-step growth method for high-performance electronic devices *ACS Nano* **6** 3624-30
[9] Ren D, Dheeraj D L, Jin C, Nilsen J S, Huh J, Reinertsen J F, Munshi A M, Gustafsson A, van Helvoort A T and Weman H 2016 New insights into the origins of Sb-induced effects on self-catalyzed GaAsSb nanowire arrays *Nano Letters* **16** 1201-9
[10] Yuan X, Caroff P, Wang F, Guo Y, Wang Y, Jackson H E, Smith L M, Tan H H and Jagadish C 2015 Antimony induced {112} A faceted triangular $GaAs_{1-x}Sb_x$/InP Core/Shell nanowires and their enhanced optical quality *Advanced Functional Materials* **25** 5300-8
[11] Yuan X, Caroff P, Wong-Leung J, Tan H H and Jagadish C 2015 Controlling the morphology, composition and crystal structure in gold-seeded $GaAs_{1-x}Sb_x$ nanowires *Nanoscale* **7** 4995-5003
[12] Yan R, Gargas D and Yang P 2009 Nanowire photonics *Nature Photonics* **3** 569-76
[13] Wallentin J, Anttu N, Asoli D, Huffman M, Åberg I, Magnusson M H, Siefer G, Fuss-Kailuweit P, Dimroth F, Witzigmann B, Xu H Q, Lars S, Deppert K and Borgström M T 2013 InP nanowire array solar cells achieving 13.8% efficiency by exceeding the ray optics limit *Science* **339** 1057-60
[14] Guo N, Hu W, Liao L, Yip S, Ho J C, Miao J, Zhang Z, Zou J, Jiang T, Wu S, Chen X and Lu W 2014 Anomalous and highly efficient InAs nanowire phototransistors based on majority carrier transport at room temperature *Advanced Materials* **26** 8203-9
[15] Yuan X, Caroff P, Wong‐Leung J, Fu L, Tan H H and Jagadish C 2015 Tunable Polarity in a III-V Nanowire by Droplet Wetting and Surface Energy Engineering *Advanced Materials* **27** 6096-103
[16] Dick K A and Caroff P 2014 Metal-seeded growth of III–V semiconductor nanowires: towards gold-free synthesis *Nanoscale* **6** 3006-21

DISTRIBUTION A: Distribution approved for public release.

Figure captions

Figure 1. (a-d) SEM images at 30° tilt view of as-grown $GaAs_xSb_{1-x}$ NW arrays with pitch size of 400 nm and Au particle diameter of 30, 50, 70 and 100 nm, respectively. (e-h) SEM images at 30° tilt view of as-grown $GaAs_xSb_{1-x}$ NW arrays with pitch size of 800 nm and Au particle diameter of 30, 50, 70 and 100 nm, respectively. The scale bars are 500 nm.

Figure 2. (a,b) TEM images of a single $GaAs_{0.94}Sb_{0.06}$ NW with (c) the HRTEM image of a selected region and diffraction pattern confirming the twin-free ZB structure of the NW.

Figure 3. Room temperature PL emission of NW arrays with pitch size of (a) 400 nm and (b) 800 nm, when the Au particle diameter is 30, 50, 70 and 100 nm, respectively.

Figure 4. Room temperature dark and light *I-V* curves of NW array photodetectors with pitch size of (a) 400 nm and (b) 800 nm, when the Au particle diameter is 30, 50, 70 and 100 nm, respectively.

Figure 5. Room temperature spectral response of NW array photodetectors with pitch size of (a) 400 nm and (b) 800 nm at 1V bias, when the Au particle diameter is 30, 50, 70 and 100 nm, respectively.

Figure 6. Simulated absorption spectra of NW arrays with pitch size of (a) 400 nm and (b) 800 nm, when the Au particle diameter is 30, 50, 70, 90 and 100 nm, respectively. (c) Simulated absorption spectra of NW arrays with pitch size of 800 nm when the Au particle diameter is ranging from 120 to 240 nm.

DISTRIBUTION A: Distribution approved for public release.

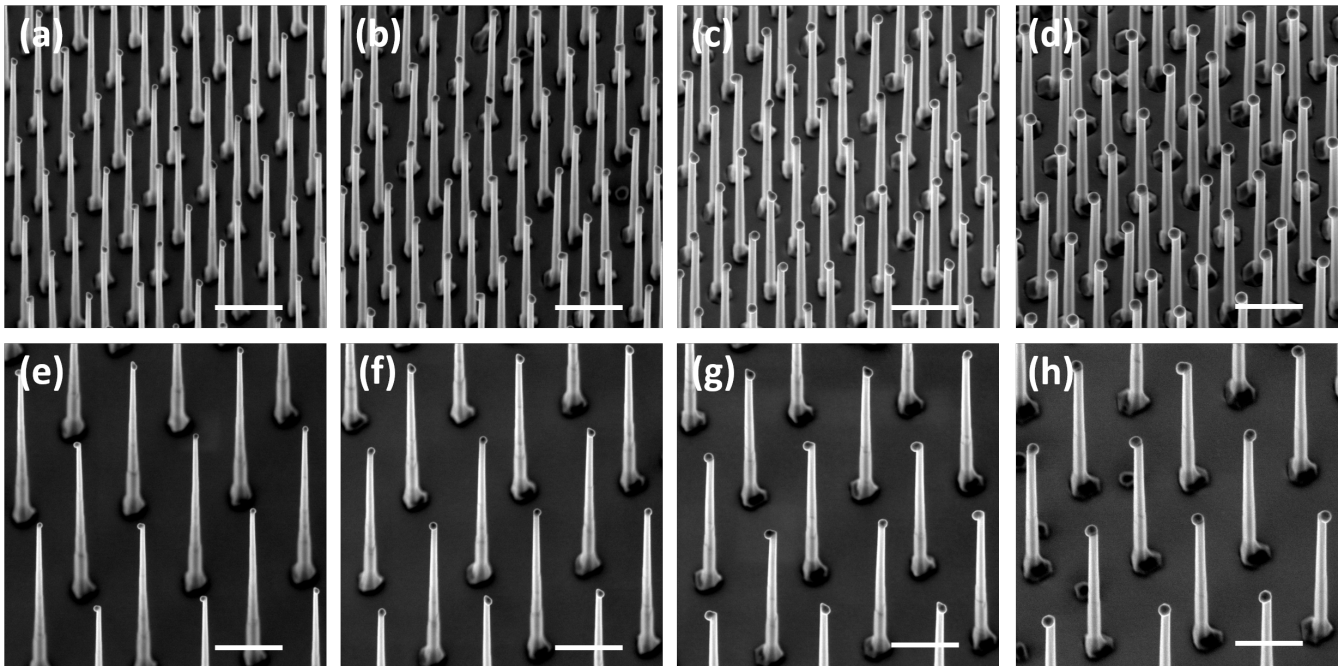

Figure 1.

DISTRIBUTION A: Distribution approved for public release.

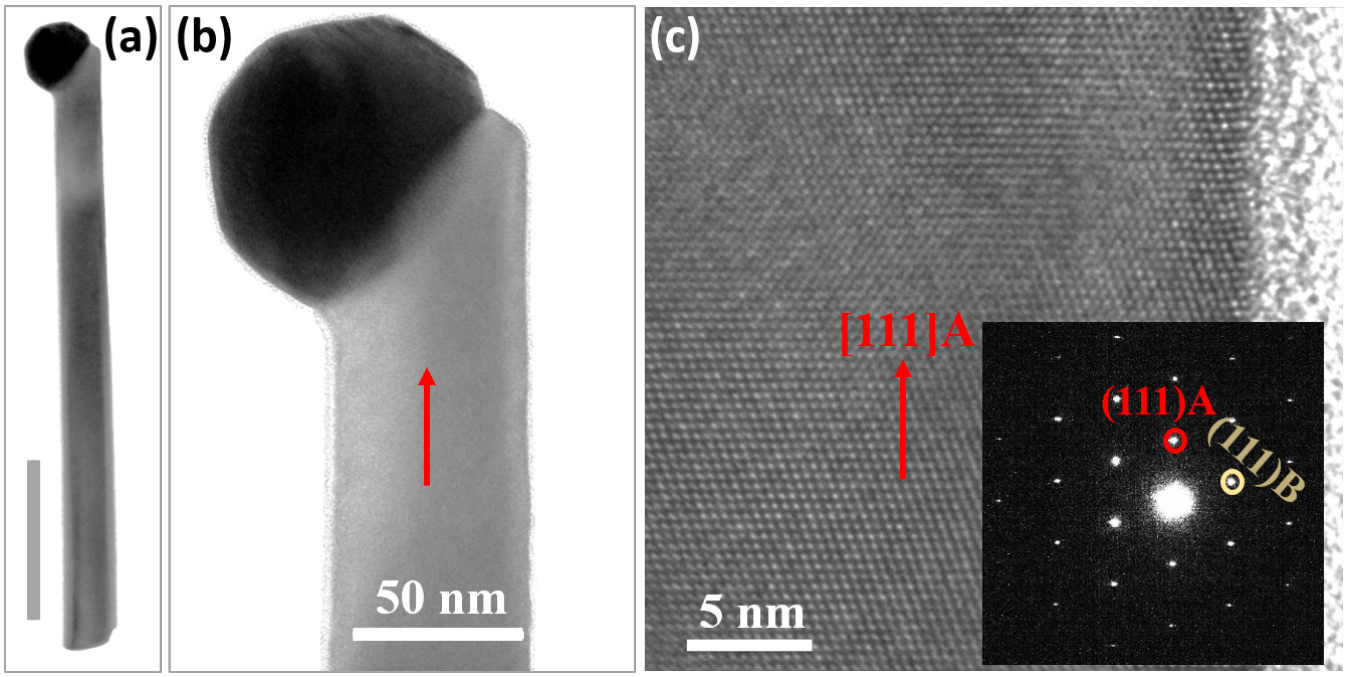

Figure 2.

DISTRIBUTION A: Distribution approved for public release.

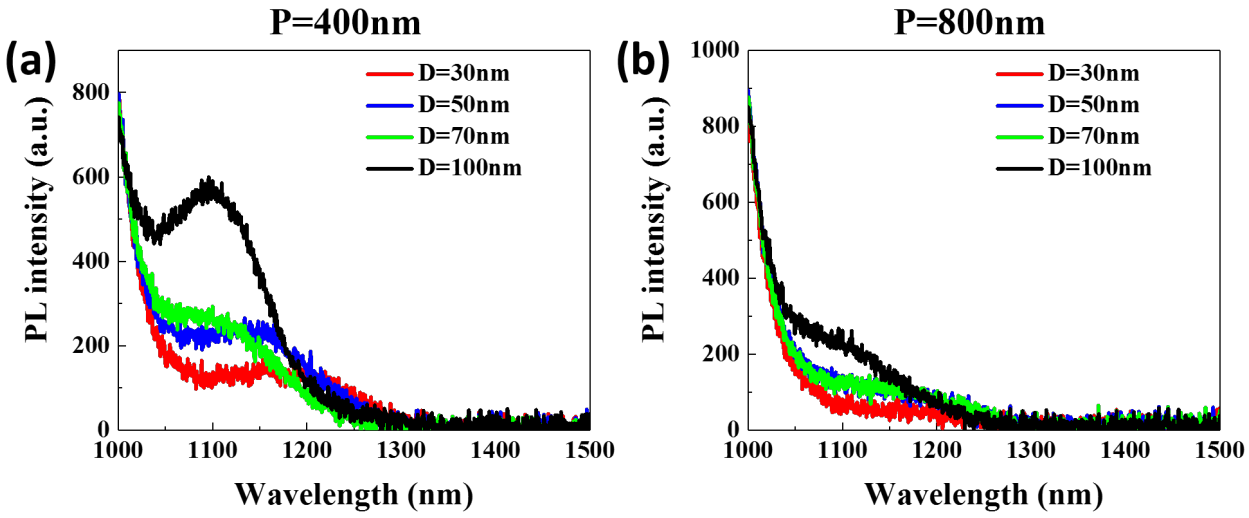

Figure 3.

DISTRIBUTION A: Distribution approved for public release.

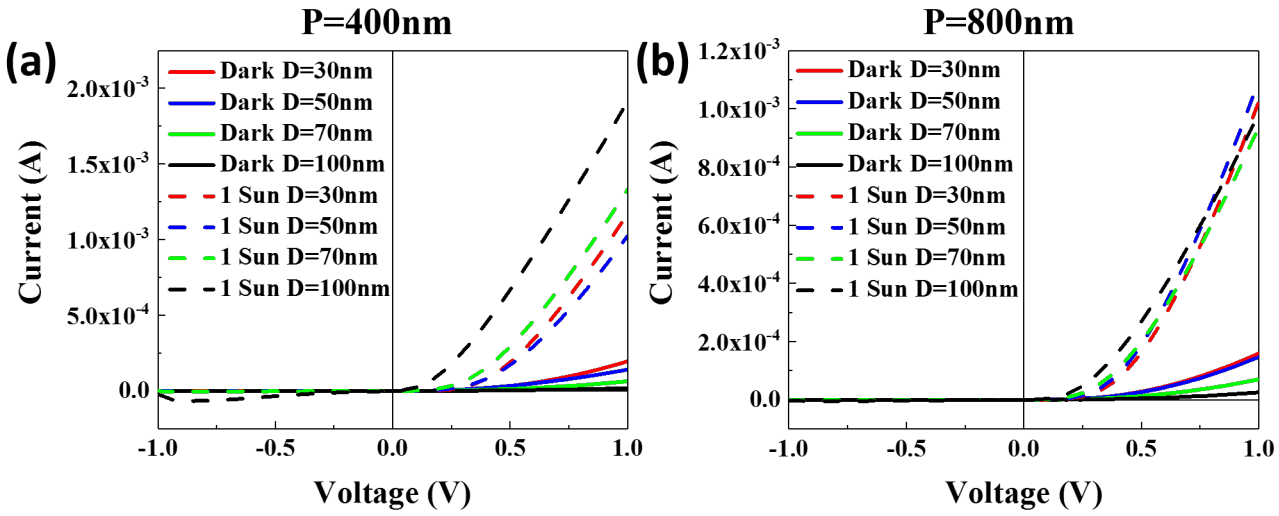

Figure 4.

DISTRIBUTION A: Distribution approved for public release.

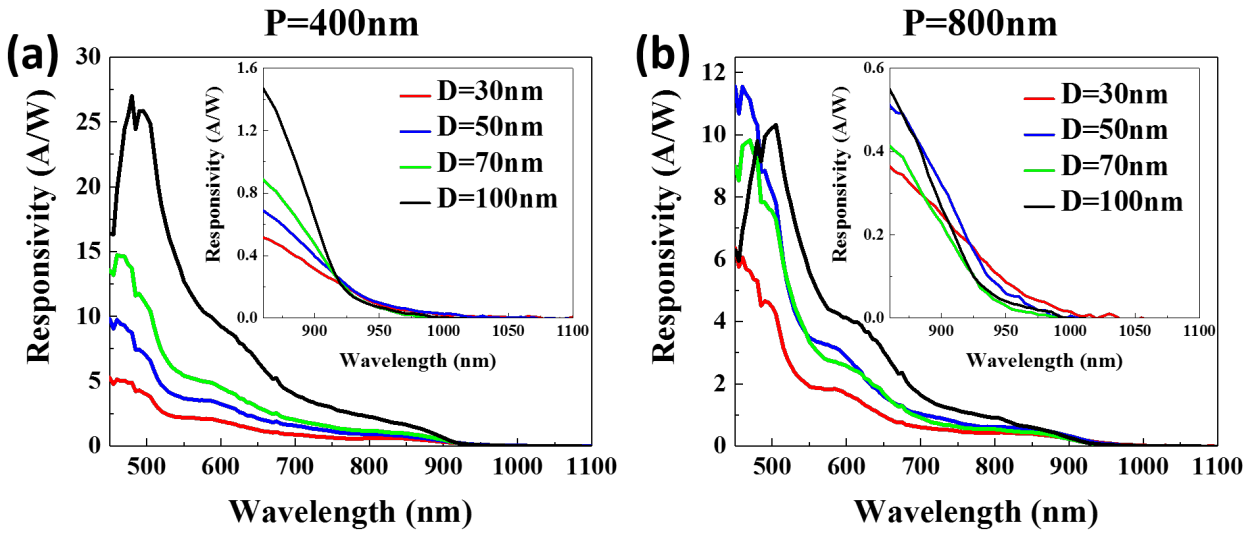

Figure 5.

DISTRIBUTION A: Distribution approved for public release.

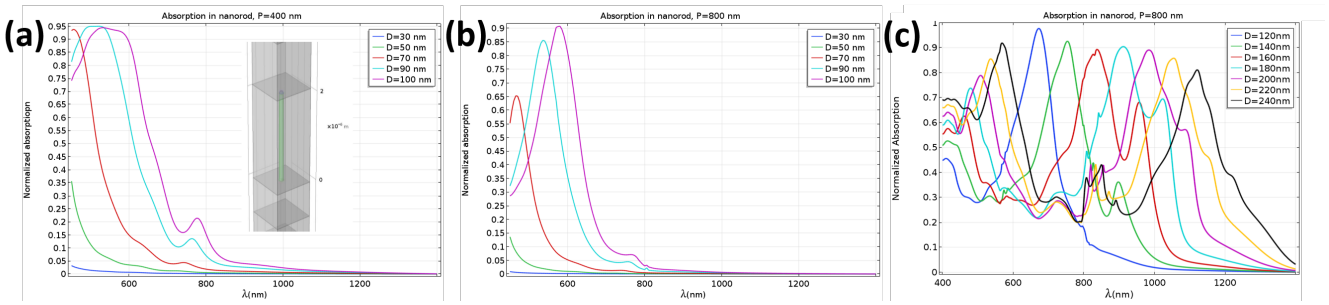

Figure 6.

DISTRIBUTION A: Distribution approved for public release.

GaAsSb/InP core-shell single nanowire infrared photodetectors

Ziyuan Li,[1] Qian Gao,[1] Xiaoming Yuan,[1,b)] Philippe Caroff,[1,c)] Monica Allen,[2] Jeffery Allen,[2] Hark Hoe Tan,[1] Chennupati Jagadish and Lan Fu[1,a)]

[1]*Department of Electronic Materials Engineering, Research School of Physics and Engineering, The Australian National University, Canberra, ACT 2601, Australia*

[2]*Air Force Research Laboratory, Munitions Directorate, Eglin AFB, FL 32542, USA*

Surface passivation of GaAsSb nanowires (NWs) is important for their performance in optoelectronic applications such as infrared photodetection. Here, the passivation effect of a ~ 12 nm epitaxial InP shell on $GaAs_{0.71}Sb_{0.29}$ NWs is experimentally analyzed. $GaAs_{0.71}Sb_{0.29}$/InP core-shell NWs were grown by metal organic vapor phase epitaxy (MOVPE) using the metal-seeded vapor–liquid–solid (VLS) growth method. After surface passivation of the InP shell, the single $GaAs_{0.71}Sb_{0.29}$/InP core-shell NW photodetector shows a responsivity of 101 A/W (@ 1.3 μm and 1.5 V) that is significantly enhanced compared to that of single $GaAs_{0.71}Sb_{0.29}$ core-only NW photodetectors (38.7 A/W). Both core-only and core-shell photodetectors show high Johnson noise and shot noise-limited detectivity of 1.6×10^{10} and 1.42×10^{10} $\mathrm{cm}\sqrt{\mathrm{Hz}}/\mathrm{W}$ at 1.3 μm and 1.5 V, respectively. Our results suggest that such devices are promising in applications of optical telecommunications.

III-V semiconductor nanowires (NWs) have been widely used in optoelectronic devices such as photodetectors,[1-3] solar cells,[4-6] light-emitting diodes (LEDs),[7-9] etc. because they have superior optical properties in light confinement, direct bandgap absorption and photosensitivity, as well as good control in bottom-up synthesis and heterostructure formation.[1] Recently, ternary $GaAs_{1-x}Sb_x$ NWs have been widely used as infrared photodetectors and logic circuits [10-12] due to their wide tunable bandgap from 870 (GaAs) to 1700 nm (GaSb) and associated flexibility in bandgap engineering.[11,13] In our previous paper, we demonstrated that $GaAs_{0.56}Sb_{0.44}$ NW-based photodetectors have good responsivity and detectivity at both 1.3 and 1.55 μm, indicating promising applications in optoelectronic integrated communication systems.[11]

a) Author to whom correspondence should be addressed. Electronic mail: lan.fu@anu.edu.au.

DISTRIBUTION A: Distribution approved for public release.

[b] Xiaoming Yuan is currently at School of Physics and Electronics, Hunan Key Laboratory for Supermicrostructure and Ultrafast Process, Central South University, 932 South Lushan Road, Changsha, Hunan 410083, P. R. China

[c] Philippe Caroff is currently at Microsoft Station Q, Delft University of Technology, Building 22, Faculty of Applied Sciences, Lorentzweg 1, 2628 CJ Delft, Netherlands

It is well known that undoped $GaAs_{1-x}Sb_x$ is always *p* type in nature because of high-concentration residual acceptors such as gallium vacancies (V_{Ga}) and gallium in antimony site (Ga_{Sb}).[10,11] However, its large surface recombination velocity (SRV) and alloy scattering lead to very low hole mobility and thus limiting the device performance.[11] Therefore, passivation is important to substantially reduce the surface state density and increase the carrier mobility for further improvement of NW-based device performance. InP shell is a good choice for passivation because of its low SRV and matched lattice to $GaAs_{1-x}Sb_x$ core.[14,15] In this work, we demonstrated the passivation effect of InP shell on $GaAs_{0.71}Sb_{0.29}$ NW core and applied the $GaAs_{0.71}Sb_{0.29}$/InP as infrared photodetectors with high photoresponse and detectivity.

Both $GaAs_{0.71}Sb_{0.29}$ core-only and $GaAs_{0.71}Sb_{0.29}$/InP core-shell NWs were grown in a horizontal flow metal organic vapor phase epitaxy (MOVPE) reactor (Aixtron 200/4). First, 40 nm Au colloids were deposited for 40 seconds on a GaAs (111)B substrate dipped into poly-Lysine for 1 min and dried with nitrogen. Trimethylgallium (TMGa), trimethylantimony (TMSb) and arsine (AsH_3) were used as precursors for the growth of $GaAs_{0.71}Sb_{0.29}$ core, while trimethylindium (TMIn) and phosphine (PH_3) were used as precursors for the InP shell growth. Hydrogen was the carrier gas for precursors and the total gas flow was 15 l/min. GaAs stems were grown for 5 min before switching to $GaAs_{0.71}Sb_{0.29}$ core growth. The growth conditions for the GaAs stem were: T = 500 °C, TMGa = 1.2×10^{-5} mol/min and AsH_3/TMGa = 23. Then the $GaAs_{0.71}Sb_{0.29}$ NW core was grown on the GaAs stem for 90 min with the growth conditions: T = 500 ºC, TMGa = 1.2×10^{-5} mol/min, AsH_3/TMGa = 1.25 and TMSb/TMGa = 0.75. Larger V/III ratio and higher temperature were used to smoothly form a radial InP shell. The optimized InP shell growth conditions were: T = 550 °C, TMIn = 0.6746×10^{-5} mol/min, V/III = 1000 and growth time *t* = 16 min. The overall Sb composition was determined by an energy dispersive x-ray

DISTRIBUTION A: Distribution approved for public release.

(EDX) spectroscopy equipped in a transmission electron microscope (TEM) for over ten NWs. The morphology of both core-only and core-shell NWs was characterized by a scanning electron microscopy (SEM), and the optical properties were assessed by room-temperature micro-photoluminescence (μ-PL) using a confocal micro-Raman system (Horiba Jobin Yvon 64000) equipped with a laser diode emitting at 532 nm.

After growth, NWs were mechanically dispersed on a 300 nm-thick SiO_2 layer that has been thermally oxidized on a p^+-Si substrate. A Raith 150 electron-beam lithography (EBL) system was used to define the electrode patterns on the single horizontal NWs.[9] Then oxygen plasma from a barrel etcher was introduced to remove the resist residue on the surface of NWs, followed by wet etching using 9% HCl for 2 min to remove the native oxide formed on the core-only NW surface and 3min40s to remove the InP shell of the core-shell NWs in the contact areas, respectively. The NWs were then metalized using electron beam evaporation and lifted off to form Ti/Au (10/220 nm) electrodes with 1.5 μm separation. The typical dark/light *I-V* curves of the NW detectors were measured by a KEYSIGHT B2902A precision source. The spectral response of the detectors was measured using the conventional amplitude modulation technique with a tungsten-halogen lamp as a white illumination source, a mechanical chopper, an Acton SpectraPro® 2300i monochromator, a Stanford SR570 low-noise current pre-amplifier and a Stanford SR830 DSP lock-in amplifier.[11] The 2-dimensional (2D) photocurrent and reflection mappings of the detectors were performed with a WITec alpha300S scanning microscopy system. Light at 532 nm from a Fianium WhiteLase supercontinuum laser was focused using a 100×, NA0.9 objective lens, and scanned across the sample using a piezo-driven sample stage. The photocurrent was detected using a similar lock-in detection system described above, and the reflected light was measured simultaneously using a confocal microscope and a Si avalanche photo-diode (APD) detector.

DISTRIBUTION A: Distribution approved for public release.

Figures 1 (a) and (b) show the SEM images of as-grown $GaAs_{0.71}Sb_{0.29}$ and $GaAs_{0.71}Sb_{0.29}$/InP NWs, respectively, which present a nearly 100% vertical yield and a tapered morphology. The insets show the magnified images of the NWs with the top Au particles. In Fig. 1(c), TEM image and EDX mappings of a typical cross-section of $GaAs_{0.71}Sb_{0.29}$/InP NWs show the hexagonal core and {112}A terminated triangular shape of InP shell. Fig. 1 (d) and (e) show the TEM images and EDX mappings of the area close to NW top and base, respectively. All these TEM mappings confirm that no In or P could be detected in the core while trace amount of Sb are found in the shell. The comparison of the PL emission of single $GaAs_{0.71}Sb_{0.29}$ and $GaAs_{0.71}Sb_{0.29}$/InP NWs at room temperature is presented in Fig. 1(f). The PL intensities of the core-only NW are amplified by 20 times for visibility. It can be clearly seen that, after the surface passivation by introducing InP shell, the PL intensity is significantly enhanced. By using the transient Rayleigh scattering spectroscopy (TRS), Yuan *et al* demonstrated that the core-only NW showed system limited lifetime of ~ 31 ps at room temperature while core-shell NW showed enhanced lifetime of ~ 100 ps at room temperature.[13] This confirms that the surface recombination velocity (SRV) is decreased due to the passivation. In the regime where surface recombination dominates the dynamics of recombination, the SRV of a NW can be calculated based on the equation as shown below:[16]

$$\frac{1}{\tau_{mc}} \cong \frac{4S}{D} \quad , \tag{1}$$

where S is the SRV and D is the NW diameter. Substituting the average diameter of 100 nm for core-only and 120 nm for core-shell into equation (1), a SRV of ~ 8.06×10^4 and 3×10^4 cm/s is obtained for core-only and core-shell, respectively, indicating decreased SRV after InP shell passivation. Moreover, both spectra exhibit a peak emission wavelength at ~ 1.35 μm, suggesting that these NWs are suitable for photodetection of the 1.3 μm telecommunication wavelength.

DISTRIBUTION A: Distribution approved for public release.

Figure 2(a) shows the SEM image of a fabricated single $GaAs_{0.71}Sb_{0.29}$/InP NW photodetector while Fig. 2(b) plots the typical dark/light *I-V* curves measured from the $GaAs_{0.71}Sb_{0.29}$ core-only and $GaAs_{0.71}Sb_{0.29}$/InP core-shell devices. Here we assume that the forward bias is applied to the electrode on the tip of the core-only and core-shell NWs. Compared with the dark currents, higher currents under illumination of a white light source (halogen lamp with a beam spot spatially covering the whole NW) were obtained, indicating that both core-only and core-shell GaAsSb NWs are good for photodetection applications. The linear and symmetrical features of the dark/light *I-V* curves of the core-only devices indicate good Ohmic contact between the electrodes and the NWs. On the other hand, core-shell devices have dark/light I-V curves that show slightly asymmetrical behavior but with significantly higher currents compared to the core-only devices as seen in Fig. 2(b). It is known that the surface states of dangling bonds exist on the GaAsSb surface and bring a large amount of non-radiative recombination centers, leading to low luminescence, carrier lifetime, carrier velocity of materials as well as electrical conductivity.[17] After the InP shell passivation, the number of surface states is decreased and thus the conductivity is increased with enhanced dark current. In addition, as demonstrated by the PL and lifetime enhancements, the addition of InP shell decreases the SRV, which can improve the carrier mobility - a key parameter for p-type semiconductor photoconductivity $\sigma_{ph} = pG\mu_p\tau_p$, where p is the hole concentration, μ_p is the hole mobility, τ_p is the lifetime of holes and G is the carrier generation rate upon photoexcitation.[11] Thus the photocurrent of our NW core-shell detector is increased as well in comparison to core-only detector. Moreover, the photocurrent value is slightly higher when the bias voltage applied to the tip of the core-shell NW. The main reason is that the GaAsSb NWs are tapered and therefor the tip's diameter is much smaller than the base and thus covered and passivated by the InP shell better than the base that is poorly covered in <112>A directions.[15] However, the etching process to remove InP shell should be well-developed that the core is exposed and contacted for carrier collection.

DISTRIBUTION A: Distribution approved for public release.

To evaluate if the photocurrent is from the NW itself or the metal/semiconductor Schottky contacts, 2D photocurrent mappings of the core-only and core-shell NW detectors were performed under a 532 nm laser excitation and a bias at positive and negative 1.5 V, respectively. As demonstrated clearly in Figure 3, the spatial distribution of the photocurrents for both core-only and core-shell NWs (as indicated by the white dotted circle) corresponds very well to that of exposed part of the NWs without contacts (as indicated by the white dotted circle in the reflection profile), unambiguously confirming that photocurrents originate from the NWs themselves based on the simple photoconductor mechanism.

To further analyze the passivation effect of the InP shell, we obtained the room temperature spectral response of both single $GaAs_{0.71}Sb_{0.29}$ core-only and $GaAs_{0.71}Sb_{0.29}$/InP core-shell NW detectors as shown in Figure 4 (a). The NW photodetector's spectral responsivity (R) was calculated using the following equation:[11]

$$R = I_{\mathrm{ph}} / P_{\mathrm{in}} \quad , \tag{2}$$

where I_{ph} is the photocurrent and P_{in} is the light power incident onto the surface of the NW. For the telecommunication wavelength of 1.3 μm, a responsivity value of 38.7 and 101 A/W at a bias voltage of 1.5 V and chopper frequency of 333 Hz was obtained for core-only and core-shell, respectively. The increased photocurrent responsivity indicates the good shell passivation. The Johnson noise and shot noise-limited detectivity is also calculated with the formula:[11]

$$D^{*} = \frac{R \bullet \sqrt{A_{\mathrm{d}}}}{\sqrt{2qI + 4kT / R_{\mathrm{d}}}}, \tag{3}$$

where R is the responsivity, A_{d} is the NW area, I is the dark current density, and R_{d} is the dynamic resistance which is defined as $R_{\mathrm{d}} = \left(dI / dV \big|_{V=0} \right)^{-1}$. The detectivity at 1.3 μm and 1.5 V is 1.6×10^{10} and $1.42\times10^{10}\,\mathrm{cm}\sqrt{\mathrm{Hz}}/\mathrm{W}$ for core-only and core-shell NW detectors, respectively. While the detectivity

DISTRIBUTION A: Distribution approved for public release.

values of both detectors' are high, the core-only devices exhibit slightly higher values due to much lower dark current. Such high responsivity and detectivity at 1.3 μm indicate promising applications for optical telecommunication/sensing systems.

The response time of the photodetectors can also be calculated from the photocurrent versus time curve. The periodic photocurrent switching corresponding to the on and off states of the light is illustrated in Fig. 4 (b) at a low chopper frequency of 14 Hz and bias voltage of 1.5 V. The response time and recovery time, defined as the time between 10% and 90% of maximum photocurrent,[18] is 6.4 ms and 9.7 ms for core-only, 3.2 ms and 5.6 ms for core-shell respectively. The core-shell detector has slight less response and recovery time, indicating a reversible and relatively faster detector response. This also confirms the passivation effect of the InP shell, leading to better device performance. However, both the spectrum response and current response of core/shell device's show higher noise than core-only's due to higher dark current.

In summary, surface passivated $GaAs_{0.71}Sb_{0.29}$/InP NWs were synthesized using MOVPE and successfully demonstrated to operate as infrared photodetectors at room temperature. Compared with $GaAs_{0.71}Sb_{0.29}$ core-only photodetectors, core-shell NW photodetectors exhibited significant improvement of infrared photoresponse at 1.3 μm. These photodetectors are promising for applications in nanoscale optical telecommunication systems and future optoelectronic integration.

The authors would like to acknowledge the support from the Air Force Office of Scientific Research (AFOSR; PO: Dr. Jermont Chen; FA2386-16-1-4076) and Australian Research Council (ARC). The authors (MSA and JWA) are thankful for the funding support through AFOSR Lab Task 17RWCOR398 (PO: Dr. K. Caster). The facility support from the Australian National Fabrication Facility (ANFF) ACT node is also acknowledged.

DISTRIBUTION A: Distribution approved for public release.

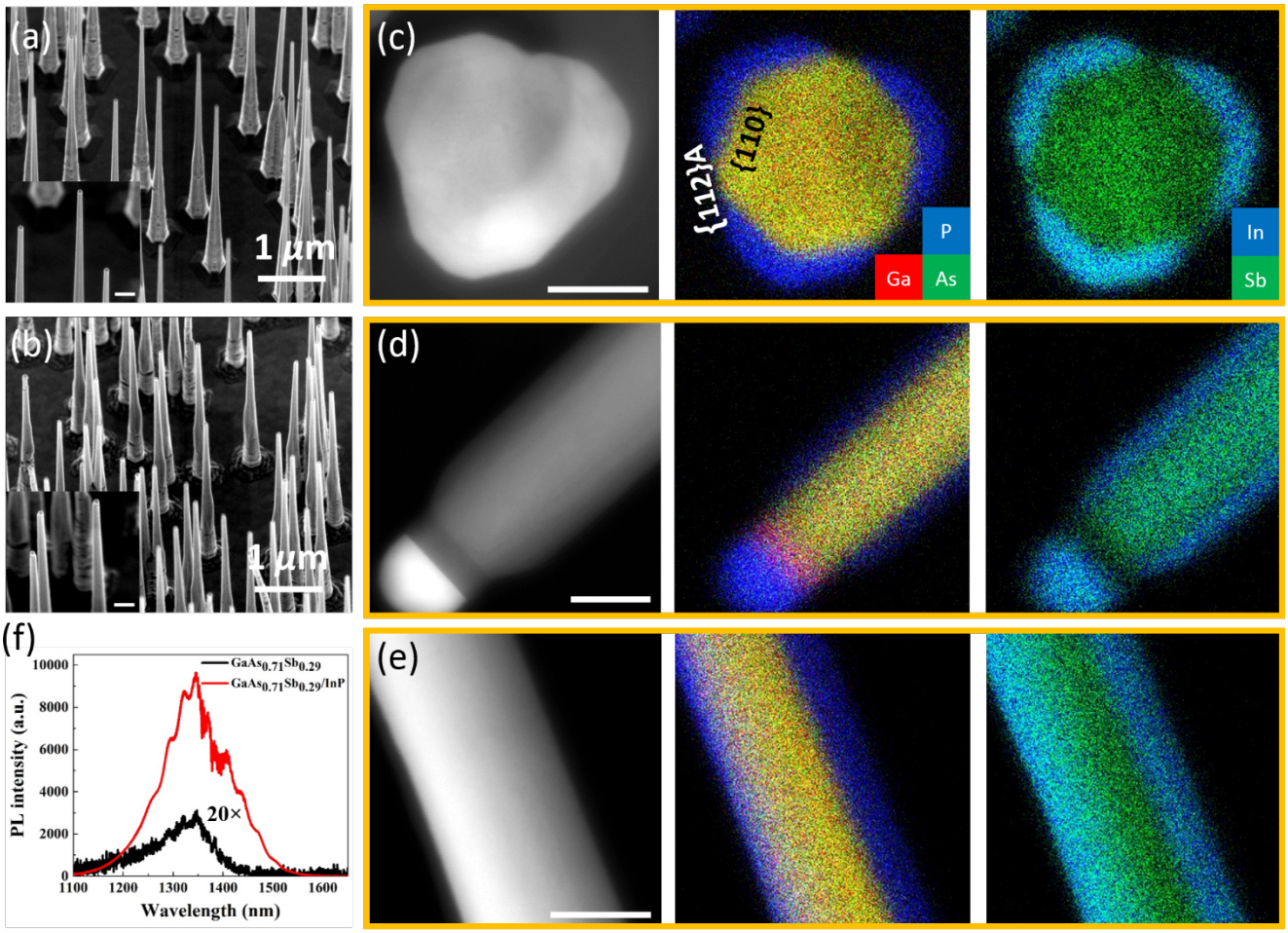

FIG. 1. (a) and (b) SEM images of as-grown $GaAs_{0.71}Sb_{0.29}$ and $GaAs_{0.71}Sb_{0.29}$/InP NWs, respectively. The insets show magnified images of the NWs with the top Au particles. Scale bars in the insets are 100 nm. (c-e) TEM images and EDX mappings of the $GaAs_{0.71}Sb_{0.29}$/InP core-shell NW. The scale bars are 50 nm. (f) Comparison of the PL emission of single $GaAs_{0.71}Sb_{0.29}$ and $GaAs_{0.71}Sb_{0.29}$/InP NWs at room temperature. The PL intensities of the core only NW are amplified by 20 times for visibility.

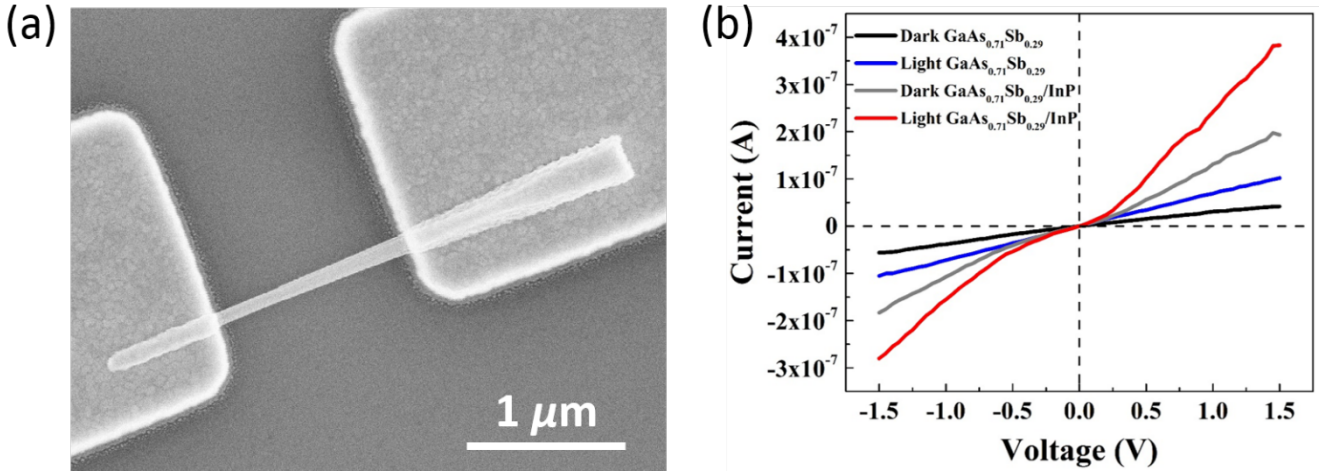

FIG. 2. (a) SEM image of a single $GaAs_{0.71}Sb_{0.29}$/InP NW photodetector. (b) I-V comparison of the $GaAs_{0.71}Sb_{0.29}$ and $GaAs_{0.71}Sb_{0.29}$/InP NW photodetectors under dark and white light conditions, respectively. In this work, the forward bias voltage is always applied on the tip.

DISTRIBUTION A: Distribution approved for public release.

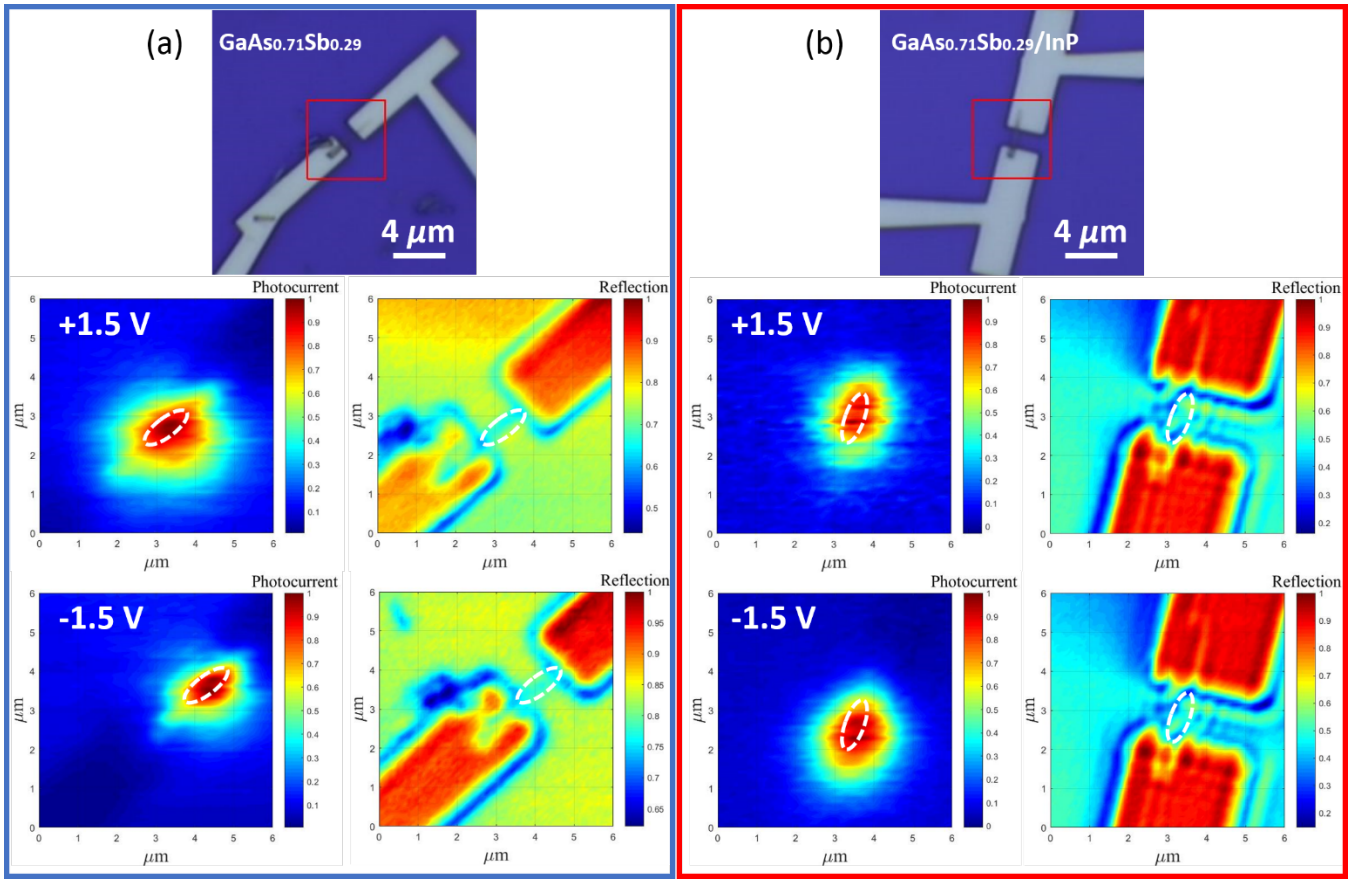

FIG. 3. Optical images, 2D photocurrent and reflection maps of the fabricated (a) $GaAs_{0.71}Sb_{0.29}$ core-only NW photodetector and (b) $GaAs_{0.71}Sb_{0.29}$/InP core-shell NW photodetector under 1.5V and -1.5V bias voltage, respectively.

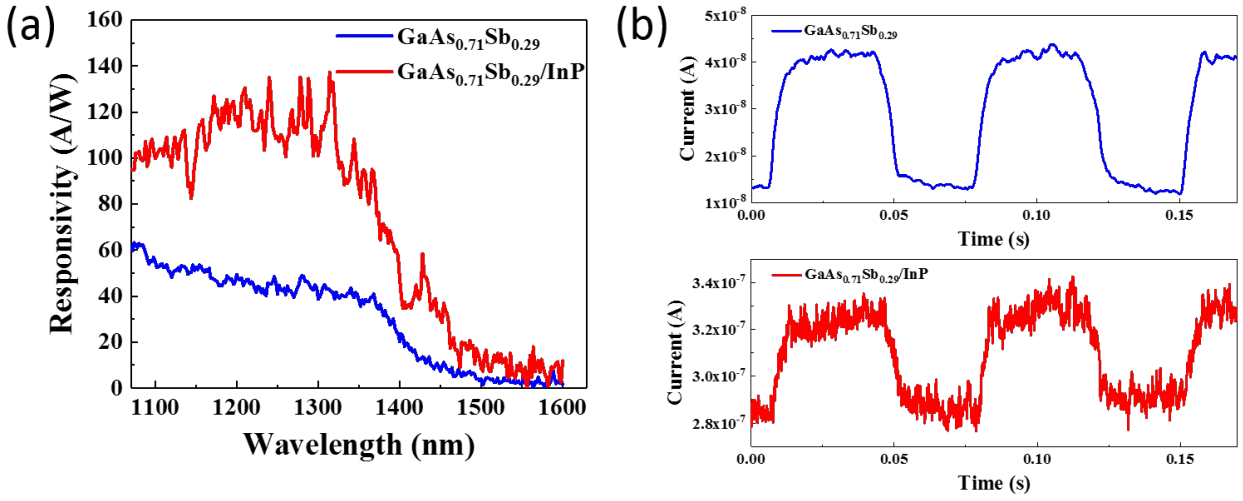

FIG. 4. (a) Spectral response of $GaAs_{0.71}Sb_{0.29}$ and $GaAs_{0.71}Sb_{0.29}$/InP photodetectors, respectively, when bias voltage = 1.5 V and chopper frequency = 333 Hz. (b) Response time of $GaAs_{0.71}Sb_{0.29}$ and $GaAs_{0.71}Sb_{0.29}$/InP photodetectors, respectively, when the chopper frequency = 14 Hz.

DISTRIBUTION A: Distribution approved for public release.

[1]Xing Dai, Sen Zhang, Zilong Wang, Giorgio Adamo, Hai Liu, Yizhong Huang, Christophe Couteau, and Cesare Soci, Nano Letters **14** (5), 2688 (2014).
[2]Tao Luo, Bo Liang, Zhe Liu, Xuming Xie, Zheng Lou, and Guozhen Shen, Sci. Bull. **60** (1), 101 (2015).
[3]Johannes Svensson, Nicklas Anttu, Neimantas Vainorius, B. Mattias Borg, and Lars-Erik Wernersson, Nano Letters **13** (4), 1380 (2013).
[4]Jeppe V Holm, Henrik I Jørgensen, Peter Krogstrup, Jesper Nygård, Huiyun Liu, and Martin Aagesen, Nature Communications **4**, 1498 (2013).
[5]Ali Nowzari, Magnus Heurlin, Vishal Jain, Kristian Storm, Ali Hosseinnia, Nicklas Anttu, Magnus T Borgström, Håkan Pettersson, and Lars Samuelson, Nano Letters **15** (3), 1809 (2015).
[6]Zhiqin Zhong, Ziyuan Li, Qian Gao, Zhe Li, Kun Peng, Li Li, Sudha Mokkapati, Kaushal Vora, Jiang Wu, and Guojun Zhang, Nano Energy **28**, 106 (2016).
[7]Satoshi Maeda, Katsuhiro Tomioka, Shinjiroh Hara, and Junichi Motohisa, Japanese Journal of Applied Physics **51** (2S), 02BN03 (2012).
[8]Ethan D Minot, Freek Kelkensberg, Maarten Van Kouwen, Jorden A Van Dam, Leo P Kouwenhoven, Valery Zwiller, Magnus T Borgström, Olaf Wunnicke, Marcel A Verheijen, and Erik PAM Bakkers, Nano Letters **7** (2), 367 (2007).
[9]Guogang Zhang, Ziyuan Li, Xiaoming Yuan, Fan Wang, Lan Fu, Zhe Zhuang, Fang-Fang Ren, Bin Liu, Rong Zhang, and Hark Hoe Tan, Nanotechnology **27** (43), 435205 (2016).
[10]Junghwan Huh, Hoyeol Yun, Dong-Chul Kim, A. Mazid Munshi, Dasa L. Dheeraj, Hanne Kauko, Antonius van Helvoort, SangWook Lee, Bjørn-Ove Fimland, and Helge Weman, Nano Letters **15** (6), 3709 (2015).
[11]Ziyuan Li, Xiaoming Yuan, Lan Fu, Kun Peng, Fan Wang, Xiao Fu, Philippe Caroff, Thomas P White, Hark Hoe Tan, and Chennupati Jagadish, Nanotechnology **26** (44), 445202 (2015).
[12]Liang Ma, Xuehong Zhang, Honglai Li, Huang Tan, Yankun Yang, Yadan Xu, Wei Hu, Xiaoli Zhu, Xiujuan Zhuang, and Anlian Pan, Semiconductor Science and Technology **30** (10), 105033 (2015).
[13]Xiaoming Yuan, Philippe Caroff, Jennifer Wong-Leung, Hark Hoe Tan, and Chennupati Jagadish, Nanoscale **7** (11), 4995 (2015).
[14]Hannah J Joyce, Callum J Docherty, Qiang Gao, H Hoe Tan, Chennupati Jagadish, James Lloyd-Hughes, Laura M Herz, and Michael B Johnston, Nanotechnology **24** (21), 214006 (2013).
[15]Xiaoming Yuan, Philippe Caroff, Fan Wang, Yanan Guo, Yuda Wang, Howard E. Jackson, Leigh M. Smith, Hark Hoe Tan, and Chennupati Jagadish, Advanced Functional Materials **25** (33), 5300 (2015).
[16]Tim Burgess, Dhruv Saxena, Sudha Mokkapati, Zhe Li, Christopher R Hall, Jeffrey A Davis, Yuda Wang, Leigh M Smith, Lan Fu, and Philippe Caroff, Nature Communications **7** (2016).
[17]Ruxue Li, Dan Fang, Jilong Tang, Xuan Fang, Xiaohua Wang, Zhipeng Wei, Shuangpeng Wang, and Fang Fang, presented at the Machinery, Materials Science and Energy Engineering (ICMMSEE 2015) Proceedings of the 3rd International Conference, 2015.
[18]Liang Ma, Wei Hu, Qinglin Zhang, Pinyun Ren, Xiujuan Zhuang, Hong Zhou, Jinyou Xu, Honglai Li, Zhengping Shan, Xiaoxia Wang, Lei Liao, H. Q. Xu, and Anlian Pan, Nano Letters **14** (2), 694 (2014).

DISTRIBUTION A: Distribution approved for public release.

Single GaAsSb/InP core-shell nanowire infrared photodetectors

Ziyuan Li[a], Qian Gao[a], Xiaoming Yuan[a], Philippe Caroff[a], Monica Allen[b], Jeffery Allen[b], Hark Hoe Tan[a], Chennupati Jagadish[a], Lan Fu*[a]
[a]Department of Electronic Materials Engineering, Research School of Physics and Engineering, The Australian National University, Canberra, ACT 2601, Australia
[b]Air Force Research Laboratory, Munitions Directorate, Eglin AFB, FL 32542, USA

ABSTRACT

III-V semiconductor nanowires (NWs) have been extensively studied for nanoscale device applications due to their small footprint, unique optical and electrical properties, and efficient strain relaxation in the formation of heterostructures. In particular, ternary $GaAs_{1-x}Sb_x$ NWs can offer wide tunable bandgaps (from 870 (GaAs) to 1700 nm (GaSb)) with associated flexibility in bandgap engineering for optoelectronic applications such as infrared photodetection. The performance of $GaAs_{1-x}Sb_x$ NW-based photodetectors can be effectively improved by surface passivation using an epitaxially grown InP shell. In our work, the passivation effect of a ~12 nm InP shell on $GaAs_{0.71}Sb_{0.29}$ NWs is experimentally investigated. $GaAs_{0.71}Sb_{0.29}$ core-only and $GaAs_{0.71}Sb_{0.29}$/InP core-shell NWs were grown by gold-seeded metalorganic vapor phase epitaxy (MOVPE) technique. While both photoluminescence (PL) spectra exhibit a peak emission wavelength at ~1.35 μm, the peak PL intensity of the $GaAs_{0.71}Sb_{0.29}$/InP NW is significantly enhanced (>60 times) compared to that of the core-only NW. After PL measurements, single NWs were mechanically transferred onto a thermally oxidized p^+-Si substrate (with 300 nm-thick SiO_2) and fabricated as photodetectors using electron-beam lithography (EBL) and Ti/Au (10/220 nm) metallization. With the surface passivation of InP shell, the single $GaAs_{0.71}Sb_{0.29}$/InP core-shell NW photodetector shows a large increase in photoresponsivity of 101 A/W @ 1.3 μm and 1.5 V compared with that of the corresponding core-only NW photodetector (38.7 A/W @ 1.3 μm and 1.5 V), indicating that GaAsSb/InP core-shell NWs are promising candidates for applications in future nanoscale integrated optical telecommunication/sensing systems.

ACKNOWLEDGEMENTS

This work has been supported by the Air Force Office of Scientific Research (AFOSR) and Australian Research Council (ARC). The Australian National Fabrication Facility (ANFF) ACT node is acknowledged for access to facilities used in this work.

*lan.fu@anu.edu.au; phone 61 2 61254060; fax 61 2 61250511.

DISTRIBUTION A: Distribution approved for public release.

GaAsSb/InP core-shell single nanowire photodetectors

Z. Y. Li[1*], Q. Gao[1], X. Yuan[1], P. Caroff[1,#], M. Allen[2], J. Allen[2], H. H. Tan[1], C. Jagadish[1], and L. Fu[1*]

[1]Department of Electronic Materials Engineering, Research School of Physics and Engineering, The Australian National University, Canberra, ACT 2601, Australia

[2]Air Force Research Laboratory, Munitions Directorate, Eglin AFB, FL 32542, USA

[#]currently at Physics Department, Cardiff University, UK

*Corresponding author: Email ziyuan.li@anu.edu.au

Email lan.fu@anu.edu.au

Abstract Summary: Single $GaAs_{0.71}Sb_{0.29}$/InP core-shell nanowires were synthesized by gold-seeded metalorganic vapor phase epitaxy (MOVPE) and fabricated as infrared photodetectors. Compared to just the core, the room temperature performance of a $GaAs_{0.71}Sb_{0.29}$ nanowire-based photodetector can be effectively improved by the surface passivation of an epitaxially grown InP shell.

Introduction: III-V semiconductor nanowires have been intensively studied for nanoscale optoelectronic device applications such as lasers, photodetectors, solar cells, due to their nanoscale size, unique optical and electrical properties, as well as efficient strain relaxation in the formation of heterostructures [1]. $GaAs_xSb_{1-x}$ nanowires are of special interest due to their wide tunable bandgaps (870 - 1700 nm) with associated flexibility in bandgap engineering for optoelectronic applications such as room temperature infrared photodetection [2, 3]. In order to further improve the performance of $GaAs_xSb_{1-x}$ nanowire-based photodetectors, surface passivation by adding an epitaxially grown shell can be promising. In this work, the passivation effect of a thin (~12 nm) InP shell on $GaAs_{0.29}Sb_{0.71}$ nanowires is experimentally analyzed. Both $GaAs_{0.71}Sb_{0.29}$ core-only and $GaAs_{0.71}Sb_{0.29}$/InP core-shell nanowires were grown by gold-seeded metalorganic vapor phase epitaxy (MOVPE) technique. With the surface passivation effect of InP shell, single $GaAs_{0.71}Sb_{0.29}$/InP core-shell nanowire photodetectors show significant performance improvement compared with the corresponding single $GaAs_{0.71}Sb_{0.29}$ core-only nanowire photodetectors.

Experimental details: The nanowires were grown on GaAs(111)B substrates with 40 nm Au colloids as seed particles, using a horizontal flow MOVPE reactor (Aixtron 200/4) [4]. Trimethylgallium (TMGa), trimethylantimony (TMSb) and arsine (AsH_3) were used as precursors for the growth of $GaAs_{0.71}Sb_{0.29}$ core, while trimethylindium (TMIn) and phosphine (PH_3) were for InP shell growth. The composition and morphology of nanowires were measured by energy dispersive X-ray (EDX) spectroscopy equipped in a transmission electron microscope (TEM) and electron scanning microscopy (SEM), respectively. Room-temperature micro-photoluminescence (μ-PL) was measured by a confocal micro-Raman/PL system (Horiba Jobin Yvon 64000) using a laser diode emitting at 532 nm. After growth, nanowires were mechanically dispersed on a thermally oxidized p^+-Si substrate (with 300 nm-thick SiO_2). Then an electron-beam lithography (EBL) system was employed to define the contact patterns on the nanowires, followed by wet etching in 9% HCl for 2 min to remove the native oxide formed on the core nanowire surface and 3 min 40 s to remove the InP shell of the core-shell nanowires in the contact areas respectively. Finally, Ti/Au (10/220 nm) electrodes were formed by metallization and lift-off. The nanowire detectors were characterized by dark/light I-V, spectral response and near-field photocurrent mapping techniques.

Results and discussion: Figure 1(a) shows the SEM image of the $GaAs_{0.71}Sb_{0.29}$/InP nanowires, which reveals a nearly 100% vertical yield and a certain degree of tapering. The comparison of the photoluminescence (PL) emission of single $GaAs_{0.71}Sb_{0.29}$ and $GaAs_{0.71}Sb_{0.29}$/InP nanowires at room temperature is presented in Fig. 1(b). The surface

DISTRIBUTION A: Distribution approved for public release.

passivation effect as a result of InP shell can be clearly seen by the significantly enhanced PL intensity. Moreover, both spectra exhibit a peak emission wavelength at ~ 1.35 μm, suggesting that these nanowires are suitable for photodetection at the 1.3 μm telecommunication wavelength. Figure 1(c) plots the typical dark/light I-V curves of a single core-shell nanowire photodetector. While it was reported that I-V curves for core-only devices show linear and symmetrical features [3], the I-V curves for the core-shell device are unsymmetrical. When forward bias is applied to the electrode on the tip of the core-shell nanowire device, both dark and light currents are significantly higher than those of core-only nanowires. A significant increase of the detector's responsivity (101 A/W) has been achieved at 1.3 μm compared to that of the $GaAs_{0.71}Sb_{0.29}$ core-only nanowire photodetectors (38.7 A/W), indicating that the InP shell is able to effectively passivate the NW surface and thus improve the photodetector's performance. Both core-only and core-shell photodetectors show high Johnson noise and shot noise-limited detectivity at 1.3 μm and 1.5 V (1.6×10^{10} and 1.42×10^{10} $\mathrm{cm}\sqrt{\mathrm{Hz}}/\mathrm{W}$, respectively).

Conclusions: In summary, we demonstrate the surface passivation effect of InP shell on $GaAs_{0.71}Sb_{0.29}$ nanowires. The nanowire photodetectors demonstrate good photoreponse at 1.3 μm with potential applications for future nanoscale integrated optical telecommunication/sensing systems.

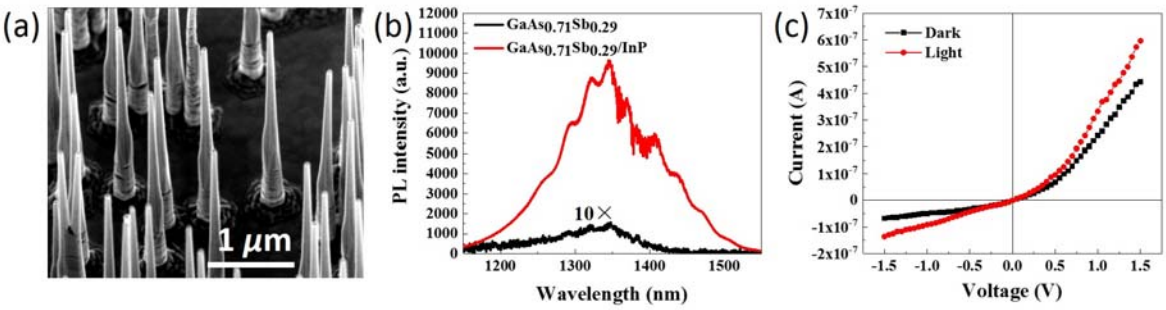

Fig. 1. (a) SEM image of as-grown $GaAs_{0.71}Sb_{0.29}$/InP nanowires used in this work. (b) Comparison of the PL emission of single $GaAs_{0.71}Sb_{0.29}$ and $GaAs_{0.71}Sb_{0.29}$/InP nanowires at room temperature. The PL intensities of the core-only nanowire are amplified by 10 times for visibility. (c) Dark and light I-V curves of a core-shell nanowire photodetector.

Acknowledgements

This work has been supported by the Air Force Office of Scientific Research (AFOSR) and Australian Research Council (ARC). The Australian National Fabrication Facility (ANFF) ACT node is acknowledged for access to facilities used in this work.

References

[1] R. Yan, D. Gargas, and P. Yang, "Nanowire photonics," Nature Photonics, vol. 3, pp. 569-576, 2009.

[2] X. Yuan, P. Caroff, J. Wong-Leung, H. H. Tan, and C. Jagadish, "Controlling the morphology, composition and crystal structure in gold-seeded $GaAs_{1-x}Sb_x$ nanowires," Nanoscales, vol. 7, pp. 4995-5003, 2015.

[3] Z. Y. Li, X. Yuan, L. Fu, K. Peng, F. Wang, X. Fu, P. Caroff, T. P. White, H. H. Tan, and C. Jagadish, "Room temperature GaAsSb single nanowire infrared photodetectors," Nanotechnology, vol. 26, pp. 445202, 2015

[4] X. Yuan, P. Caroff, F. Wang, Y. Guo, Y. Wang, H. E. Jackson, L. M. Smith, H. H. Tan, and C. Jagadish, "Antimony induced {112} A faceted triangular $GaAs_{1-x}Sb_x$/InP Core/Shell nanowires and their enhanced optical quality," Advanced Functional Materials, vol. 25, pp. 5300-5308, 2015.

DISTRIBUTION A: Distribution approved for public release.

Room temperature GaAsSb array photodetectors

Ziyuan Li[1], Simeon Trendafilov[2], Monica Allen[2], Jeffery Allen[2,*], Ahmed Alabadla[1], Qian Gao[1], Xiaoming Yuan[1,3], Inseok Yang[1], Philippe Caroff[1,4], Hark Hoe Tan[1], Chennupati Jagadish[1] and Lan Fu[1,*]

[1]*Department of Electronic Materials Engineering, Research School of Physics and Engineering, The Australian National University, Canberra, ACT 2601, Australia*
[2]*Air Force Research Laboratory, Munitions Directorate, Eglin AFB, FL 32542, USA*
[3]*School of Physics and Electronics, Hunan Key Laboratory for Supermicrostructure and Ultrafast Process, Central South University, 932 South Lushan Road, Changsha, Hunan 410083, P. R. China*
[4]*Microsoft Station Q, Delft University of Technology, Building 22, Faculty of Applied Sciences, Lorentzweg 1, 2628 CJ Delft, Netherlands*

Email: jeffery.allen.12@us.af.mil, lan.fu@anu.edu.au

***Abstract*—GaAsSb nanowire arrays were grown by gold-seeded metalorganic vapor phase epitaxy (MOVPE) and fabricated into photodetector devices. The array photodetectors operate at room temperature with tunable resonance peaks varying with the array geometry. These devices are promising for multispectral photodetector applications.**

Keywords—GaAsSb, III-V semiconductor, nanowire, VLS, photodetector

I. Introduction

III-V semiconductor nanowires (NWs) have attracted increasing attention in recent years due to their small footprint, direct bandgap, unique optical and electrical properties as well as flexibility to create heterostructures. In particular, ternary semiconductor NWs such as GaAsSb NWs have wide tunable bandgap ranging from 870 (GaAs) to 1700 nm (GaSb), which are promising photodetector candidates for integrated optical telecommunication systems [1-3]. Currently, most of the GaAsSb NWs are grown based on metal-catalyzed or self-catalyzed vapor-liquid-solid (VLS) technique [4, 5]. In our work, the NWs were grown by gold-seeded VLS technique with a SiO_2 mask to accurately define the NW size and position as well as to suppress parasitic growth. We investigated the impact of the gold-seed diameter on the NW morphology, optical properties and photodetection performance. The seed diameter was controlled through the selective-area lift-off of a gold thin film using electron-beam lithography (EBL). The photoconductive devices based on such NW arrays exhibit high responsivity and tunable resonances, indicating their promising application for the next-generation multispectral photodetection systems.

II. Experimental Details

GaAsSb NW arrays were grown using a horizontal flow metalorganic vapor phase epitaxy (MOVPE) reactor (Aixtron 200/4) at 100 mbar based on the gold-seeded VLS technique. In order to obtain gold disks with different diameters, a 30 nm SiO_2 layer was first deposited on a p-type (111)A GaAs substrate by using plasma-enhanced chemical vapor deposition (PECVD), followed by EBL patterning to define the hole diameter ranging from 30 to 100 nm and array pitch of 400 and 800 nm respectively. Then wet chemical etching was performed to open the holes in the SiO_2 layer followed by electron-beam evaporation of a 17 nm gold layer and a lift-off process. After that, the substrate was loaded into the reactor where GaAsSb NW arrays were grown at 500 °C with trimethylgallium (TMGa), trimethylantimony (TMSb) and arsine (AsH_3) as precursors for Ga, Sb and As, respectively. The morphology of GaAsSb NW arrays were characterized by scanning electron microscopy (SEM) and their optical properties were assessed by room-temperature micro-photoluminescence (μ-PL).

After growth, the NW arrays were fabricated into photodetectors through processes of photoresist planarization, barrel etching using oxygen plasma to expose the nanowire tips, wet etching to remove the native oxide, transparent conductive oxide (e.g. indium tin oxide (ITO)) deposition on front side and metal contact deposition on the back side. The typical dark/light *I-V* curves of the NW detectors were measured by a KEITHLEY 2420 SourceMeter® under a light source provided by a 1 sun solar simulator. The photocurrent spectral response of the detectors was measured using the conventional amplitude modulation technique with a white illumination source, a mechanical chopper, a monochromator, a low-noise current pre-amplifier and a lock-in amplifier.

III. Results and Discussion

Figure 1 shows the SEM image of an as-grown GaAsSb NW array with pitch size (P) of 400 nm and gold particle diameter (D) of 100 nm. The NWs reveal a nearly 100% vertical yield. When D is small (e.g., 30 nm), the NWs show a certain degree of tapering due to a large simultaneous lateral growth. For the NWs with larger diameter (as result of larger gold particle size), less tapering but slightly shorter length were observed.

DISTRIBUTION A: Distribution approved for public release.

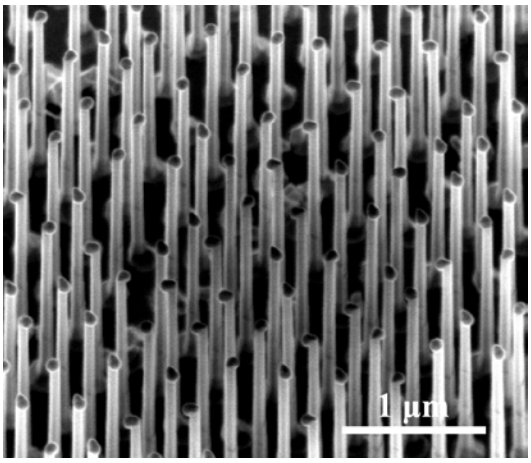

Figure 1. SEM image of an as-grown GaAsSb array with pitch size (P) of 400 nm and gold-seed diameter (D) of 100 nm.

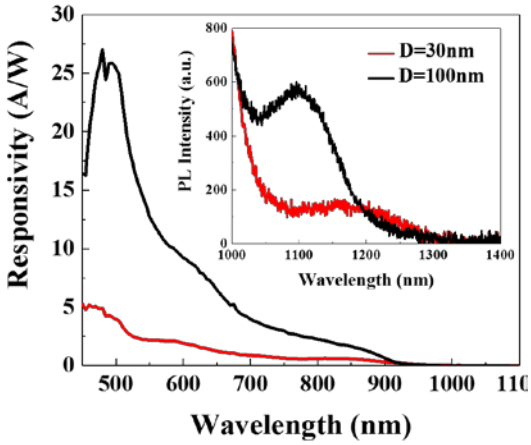

Figure 2. Photoresponse of GaAsSb NW array based photodetectors with P of 400 nm and D of 30 and 100 nm, respectively. The inset shows the PL spectra of the corresponding NW arrays.

The inset of Figure 2 presents the PL spectra of GaAsSb NW arrays with P of 400 nm and D of 30 and 100 nm, respectively. As clearly seen, the NW array with D=100 nm shows an apparent peak at wavelength of ~ 1100 nm with the highest PL intensity, while the NW array with D=30 nm shows much lower PL peak intensity with a red-shifted band gap, which may be due to the slightly increased Sb composition, decreased material volume or degraded material quality. The significantly enhanced PL signal below 1000 nm was demonstrated to be from the GaAs substrate.

To characterize the performance of the NW array photodetectors, dark/light *I-V* characteristics and photocurrent spectra were first measured. Figure 2 presents the photocurrent response of the NW array photodetectors under a bias voltage of 1 V. It can be seen that larger D leads to higher photocurrent response consistent with the PL results. In particular, such GaAsSb NW arrays show a strong resonance in the wavelengths much shorter than the NW bandgap, with an increased blue shift with the decrease of NW diameter. This is because that NWs exhibit strong waveguiding properties and will efficiently couple incident light to resonant modes supported in the NWs. Since our GaAsSb NWs have relatively small diameters, short wavelength light can be easily coupled to strong resonance modes, leading to significantly enhanced photoresponse, corresponding well with the simulated results using COMSOL Multiphysics. The responsivity of the NW array with D of 100 nm can reach as high as 27 A/W at the peak wavelength of 480 nm.

IV. Conclusions

In summary, GaAsSb NW arrays with tunable diameter and spacing were synthesized using MOVPE and fabricated as room temperature photodetectors. By engineering the diameter of the gold-seeds, GaAsSb NWs showed tunable morphology and photodetection performance. Moreover, the GaAsSb NW array photodetectors show very strong resonances in the visible wavelength range, leading to high responsivity. It indicates that by further design and fabrication of NW arrays with different geometries (diameter and spacing), it is promising to achieve multispectral photodetection with a wide spectral tunability highly desirable for a broad range of applications.

Acknowledgment

The authors would like to acknowledge the support from the Air Force Office of Scientific Research (AFOSR) (PO: Dr. J. Chen; FA2386-16-1-4076) and Australian Research Council (ARC). The authors (MSA and JWA) are thankful for the funding support through AFOSR Lab Task 17RWCOR398 (PO: Dr. K. Caster) and Air Force Research Laboratory (AFRL) Munitions Directorate Chief Scientist Venture fund (Dr. D. Lambert). The facility support from the Australian National Fabrication Facility (ANFF) ACT node is also acknowledged.

References

[1] J. Huh, H. Yun, D.-C. Kim, A. M. Munshi, D. L. Dheeraj, H. Kauko, A. T. van Helvoort, S. Lee, B.-O. Fimland, and H. Weman, "Rectifying single GaAsSb nanowire devices based on self-induced compositional gradients," Nano Letters, vol. 15, no. 6, pp. 3709-3715, 2015.

[2] Z. Li, X. Yuan, L. Fu, K. Peng, F. Wang, X. Fu, P. Caroff, T. P. White, H. H. Tan, and C. Jagadish, "Room temperature GaAsSb single nanowire infrared photodetectors," Nanotechnology, vol. 26, no. 44, pp. 445202, 2015.

[3] L. Ma, X. Zhang, H. Li, H. Tan, Y. Yang, Y. Xu, W. Hu, X. Zhu, X. Zhuang, and A. Pan, "Bandgap-engineered GaAsSb alloy nanowires for near-infrared photodetection at 1.31 μm," Semiconductor Science and Technology, vol. 30, no. 10, pp. 105033, 2015.

[4] D. Ren, D. L. Dheeraj, C. Jin, J. S. Nilsen, J. Huh, J. F. Reinertsen, A. M. Munshi, A. Gustafsson, A. T. van Helvoort, and H. Weman, "New insights into the origins of Sb-induced effects on self-catalyzed GaAsSb nanowire arrays," Nano Letters, vol. 16, no. 2, pp. 1201-1209, 2016.

[5] X. Yuan, P. Caroff, J. Wong-Leung, H. H. Tan, and C. Jagadish, "Controlling the morphology, composition and crystal structure in gold-seeded $GaAs_{1-x}Sb_x$ nanowires," Nanoscale, vol. 7, no. 11, pp. 4995-5003, 2015.

[6] K. A. Dick, and P. Caroff, "Metal-seeded growth of III–V semiconductor nanowires: towards gold-free synthesis," Nanoscale, vol. 6, no. 6, pp. 3006-3021, 2014.

DISTRIBUTION A: Distribution approved for public release.

[7] X. Yuan, P. Caroff, J. Wong-Leung, L. Fu, H. H. Tan, and C. Jagadish, "Tunable polarity in a III–V nanowire by droplet wetting and surface energy engineering," Advanced Materials, vol. 27, no. 40, pp. 6096-6103, 2015.

DISTRIBUTION A: Distribution approved for public release.